arXiv:astro-ph/0103264v1 16 Mar 2001

# DEUTERATED AMMONIA IN GALACTIC PROTOSTELLAR CORES

Ronak Y. Shah[1]
Email: shah4@astro.uiuc.edu

AND

Alwyn Wootten
Email: awootten@nrao.edu

National Radio Astronomy Observatory, Charlottesville, VA 22903
*Draft version February 1, 2008*

## ABSTRACT

We report on a survey of $NH_2D$ towards protostellar cores in low–mass star formation and quiescent regions in the Galaxy. Twenty–three out of thirty-two observed sources have significant ($\gtrsim 5\sigma$) $NH_2D$ emission. Ion–molecule chemistry, which preferentially enhances deuterium in molecules above its cosmological value of $1.6 \times 10^{-5}$ sufficiently explains these abundances. $NH_2D/NH_3$ ratios towards Class 0 sources yields information about the "fossil remnants" from the era prior to the onset of core collapse and star formation. We compare our observations with predictions of gas–phase chemical networks.

*Subject headings:* Molecular Processes; ISM: abundances; ISM: general; ISM: clouds; ISM: molecules; ISM:deuterium; radio lines: ISM

## 1. INTRODUCTION

Deuterium in molecules is enhanced above the cosmological [D]/[H] value of $1.6^{+0.14}_{-0.19} \times 10^{-5}$ (Linsky et al. 1995) by several orders of magnitude in the cold environs of the interstellar medium (ISM). Two theoretical pathways can account for the abundance of these deuterated molecules. Deuterium binds more strongly in molecules than do less massive hydrogen atoms, especially at low temperatures, in gas–phase reactions between parent species and e.g. $H_3^+$ and $H_2D^+$ (Dalgarno & Lepp 1984; Watson 1974) and other similar molecular ions in dense ($n > 10^4 \text{cm}^{-3}$) gas. The qualitative understanding that reactions specifically with $H_3^+$ and $H_2D^+$ have been enhanced by recent detections (Geballe & Oka 1996; Stark, et al. 1999). Their abundances are consistent with requirements of gas–phase ion–molecule chemistry predictions of most species, including deuterium isotopes. Reactions on grains will also contribute to deuterium enhancements. Deuteration has a smaller activation energy than does hydrogenation on grain surfaces. Additionally the more massive deuterium will desorb less quickly from grain surfaces than hydrogen, increasing the interaction time for potential grain–induced deuteration (Tielens 1983). Such predictions are considered important for the high fractionation ($\sim 10^{-2}$) observed for $HDCO/H_2CO$ (Loren & Wootten 1985), $NH_2D/NH_3$ (Walmsley et al. 1987), and $CH_3OD/CH_3OH$ (Mauersberger et al. 1988) towards the hot core Orion-KL. In such regions, high temperatures quench the ion–molecule deuterium fractionation reactions by rapid destruction of $H_2D^+$ and faster reactions (lower energy barriers) for more abundant species. High observed deuterium fractions towards these sources provide a chemical "fingerprint" of the physical conditions in the pre–protostellar gas. Comparisons of deuterated molecules to their more abundant isotopes may, then, provide meaningful insight into the evolution of the ISM.

Deuterated ammonia, $NH_2D$, is a useful probe of protostellar sources because (1) it can be easily compared to $NH_3$, a well–used tracer of temperature and dense gas condesations in the ISM; (2) it possesses easily observable millimeter transitions; (3) it has hyperfine components that can be easily resolved and used to estimate column density; and (4) its abundance can be compared with chemical models which predict variations with temperature, density and evolutionary state. $NH_2D$ was first observed by Turner et al. (1978) in Sgr B2 and Rodriguez–Kuiper et al. (1978) in Orion KL. These observations of hot core regions yielded ammonia deuterium fractionation levels, $NH_2D/NH_3$, of order a few times $10^{-3}$, significantly higher than the local ISM [D]/[H] value of $1.6 \times 10^{-5}$. Walmsley et al. (1987) suggested that longer time-scales for deuterium interaction on grain surfaces (versus that of lighter hydrogen atoms) can generate larger deuterated molecular abundances. The high temperatures in these cores sublimate or photo-evaporate grain mantles, providing the high observed $NH_2D/NH_3$ levels. Olberg et al. (1985) investigated this phenomenon in the colder, less evolved sources L183 and towards the $NH_3$ column density peak in TMC1, TMC1 $NH_3$, where low temperatures minimize any surface contributions and gas–phase chemistry dominates molecule formation. They found $NH_2D/NH_3$(L183)=0.05, but only an upper limit towards TMC1 $NH_3$. Tiné et al. (2000) revisit the difference in ammonia fractionation for L183 and TMC1. They find $NH_2D$ detections towards both sources, with L183 ($NH_2D/NH_3 \sim 0.1$) having 5 times the ammonia fractionation level of TMC1 ($NH_2D/NH_3 = 0.02$). Their gas–phase network based on the reaction rates of Millar et al. (1991) sufficiently explains the abundances and fractionation of ammonia. Saito et al. (2000) invoke grain processes to differentiate star–filled and star–less ammonia cores with and without $NH_2D$ detections, respectively. They made this conclusion despite the fact that Saito et al. (2000) measured the

---

[1] Current Address: University of Illinois at Urbana-Champaign, 1002 W. Green Street, Urbana, IL 61801

strong fractionation towards L183, with a value similar to ours and Tine et al. L183 is a well known starless core which lacks any source of radiation to sublimate grains. Some of the discrepancy in the interpretation of the origin of $NH_2D$ may result from the source samples. The listed studies have concentrated on either too few sources or sources over a small range in physical conditions.

We present in this paper an experiment to address the deuterium enhancements of ammonia, $NH_2D/NH_3$, towards dark cores and Class 0 sources. The former are often termed "pre–protosteller" since most do not possess strong continuum detectable by instruments such as *IRAS*. In such environs, ion–molecule chemistry fractionates neutrals and ions such as ammonia and $HCO^+$ (Wootten 1987) and dominates surface deuteratated components desorbed back into the ISM. Most of the grain ice mantles remain frozen since the ambient temperatures are significantly less than 90 K, the sublimation temperature of the major ice constituent, $H_2O$. Class 0 sources are cold dense cores with spectral energy distributions (SEDs) peaked in the sub-millimeter ($T_D \sim 20 - 50$ K) and highly collimated outflows (André, Ward-Thompson, & Barsony 1993). Blake et al. (1995) showed that Class 0 sources such as IRAS4 contain a large number of hydrogenated species and long–chain molecules that can only be produced by grain catalyzation. Thus, Class 0 sources represent an ideal location for separating gas–phase effects from grain chemistry. The $NH_2D/NH_3$ ratio of these sources will reflect what, if any, additional deuteration has occured on the grains.

Our observations of $NH_2D$ also reveal that four (and possibly six) sources possess asymmetric line profiles. One does not expect to see such complex line profiles from relatively low abundance (and, therefore, low optical depth) species such as $NH_2D$. Line–of–sight self–absorption or kinematic effects (e.g. multiple cores within the telescope beam) can account for such a line profile. In this work, we assert that gas–phase chemistry adequately accounts for observed deuterium enhancements in ammonia. We present a radiative transfer analysis using (multi-layer) microturbulent models in §3, and discuss how ion–molecule reactions can, in fact, effectively explain the observations, including self–absorbed profiles in section §5. We discuss our main conclusions in section §6.

## 2. OBSERVATIONS

### 2.0.1. *The $NH_2D$ molecule*

$NH_2D$ is a slightly asymmetric top molecule whose rotational levels are split by inversion doubling, as in its more well studied symmetric isotopomer, $NH_3$, but the asymmetry mixes the rotation and inversion. The primary dipole moment, $\vec{\mu_c} = 1.4652$ D, induces rotation–inversion transitions which are in turn split by the $^{14}N$ nuclear quadrupole moment into five hyperfine components (Bester et al. 1983). The inversion–split $1_{01}$ and $1_{11}$ levels, corresponding to the $\mu_c$ dipole moment, produce a symmetric and anti–symmetric transition, one at 85.926263 GHz (ortho–$NH_2D$; $v = 0 \rightarrow 1$) and the other at 110.153599 GHz (para–$NH_2D$; $v = 1 \rightarrow 0$) (see Table 1). The relative nuclear statistical weights taken from

Bester et al. (1983) favor the para–$NH_2D$ transition by a factor of 3. As in ammonia, one can compute the optical depths and column densities using ratios of the hyperfine transitions (Mangum, Wootten, & Mundy 1992; Ho & Townes 1983). A weaker dipole moment, $\vec{\mu_a} = -0.1848$ D, produces pure rotational transitions within a given inversion level. It is responsible for the ground state transitions, $J = 1_{01} \rightarrow 0_{00}$ levels at 332.82251 GHz ($v = 0$) and 332.78189 GHz ($v = 1$).

### 2.1. *NRAO 12–meter Observations*

We observed the 85.93GHz $J_{K_{-1}K_1} = 1_{11}^a \rightarrow 1_{01}^s$ and 110.15 GHz $J_{K_{-1}K_1} = 1_{11}^s \rightarrow 1_{01}^a$ rotation–inversion transitions of $NH_2D$ using the NRAO 12 meter[2] telescope at Kitt Peak, Arizona (Figures 1, 2, and 3). The data are from several epochs, mostly dating from 1987 September, but a fair portion from 1997 September, using both the filter banks and the hybrid digital spectrometer. The recent data set was observed with a two–channel SIS junction receiver tuned to receive signals in a single side–band. Each channel measured orthogonal linear polarizations. We utilized two banks of filters, 100 kHz and 250 kHz, each consisting of 256 channels, resulting in 0.27 km s$^{-1}$and 0.68 km s$^{-1}$per channel resolution. We used the hybrid spectrometer in the two–IF mode with 12.5 MHz bandwidth and 512 channels per IF, resulting in a spectral resolution of 24.4 kHz or 0.131km s$^{-1}$; both linear polarizations were averaged. All data were obtained in frequency switched mode, at a switching interval of 2.5 MHz. The excellent quality of the high resolution data from the hybrid spectrometer motivated us to use it exclusively for our analysis presented here. Filter bank data were generally used to diagnose any systematic problems.

Sky dip measurements indicated zenith opacities of 0.01 to 0.4 when few clouds were apparent. The system temperatures varied between 180 and 300 K for all observations reported here. Calibration was achieved by the synchronous detection of an ambient temperature absorber and the sky. The observed line intensities were corrected for forward scattering and spillover efficiency $\eta_{fss} = 0.68$ to place the data on a $T_R^*$ scale. Column density calculations require an additional main beam brightness correction of $\eta_m^* = 0.95$. The beamsize of the 12m at 86 GHz is 90$''$, and 70$''$ at 110 GHz. Regular pointing checks performed with planets indicated a positional accuracy better than 5$''$.

### 2.2. *CSO Observations of $NH_2D$*

We also report on the detection of the fundamental transition of $NH_2D$, $J = 1_{01} \rightarrow 0_{00}$, at 332.782 GHz (Ortho) and 332.822 GHz (Para), towards the dense core L1689N with the Caltech Submillimeter Observatory (CSO). The data were observed in orthogonal linear polarizations. The 1024–channel 50MHz acousto–optical spectrometers were

---

used. The data were position switched with $30'$ east or west offsets. The beamwidth at 333 GHz is $20''$ and the main beam efficiency, determined from planet observations, is 67% at 345 GHz.

### 2.3. *NRAO 140–foot Observations*

Observations of the ammonia transitions were made during 1998 June at the 43m telescope of the NRAO in Green Bank, West Virginia (Figure 5). The $(J, K) = (1, 1)$ (23.694506 GHz) and $(J, K) = (2, 2)$ (23.722634 GHz) transitions were observed to sensitive limits in all of our sources. All of the data were observed in orthogonal linear polarizations. The 1024 channel Mark IV autocorrelator gave a spectral resolution of 0.25 km s$^{-1}$ per channel. The data were frequency switched at an interval of 2.5 MHz. The variation of gain with elevation was reduced by use of the lateral focusing stage. The beamwidth at 23.7 GHz is $\sim 1'$ and the beam efficiency is 30%. This beam width is similar to that of the 12–meter observations. Thus, differential beam dilution is not considered when comparing the NH$_2$D and NH$_3$ column densities, assuming that both isotopes emit from similar volumes of gas. Line intensities are measured in units of T$_R^*$. The forward scattering and spillover efficiency, $\eta_{\text{fss}}$, is 0.63 (Loren, Evans, and Knapp 1979).

### 3. RESULTS

#### 3.1. NH$_3$ *and* NH$_2$D

We determined column densities for both NH$_3$ and NH$_2$D using a microturbulent radiative transfer model. We utilize H$_2$CO as a measure of source physical conditions. This explictly assumes that H$_2$CO and ammonia overlap. In general, H$_2$CO is excited in more dense regions than NH$_3$. Thus, temperature estimates from both species may not be cospatial in a given source. With this caveat in mind, we discuss below how physical conditions were determined.

#### 3.1.1. *Estimates of Source Physical Conditions*

Chemical models predict significant variations of molecular abundances with density, temperature, and evolutionary state of the cloud. We model the temperature and density structure of each source using NH$_3$ observations and formaldehyde observations from Wootten et al. (2001). For clarity we discuss some issues involved with H$_2$CO radiative transfer modeling below. H$_2$CO, an asymmetric rotor molecule, is an important probe of molecular cloud physical conditions because of:

- a large number of transitions closely spaced in frequency but well separated in energy, possessing a coupled sensitivity to kinetic temperature *and* volume density when measured through appropriately chosen line ratios.

- a large, uniform, and ubiquitous abundance in the ISM (Mangum, Wooten, Wadiak & Loren 1990).

- multiple transitions through only a few receiving systems, minimizing calibration uncertainties.

One must compare the various transitions to determine if an isothermal, iso–density cloud model or one with more elaborate physical conditions is necessary to reproduce the observed H$_2$CO transitions.

Several steps are needed to determine basic physical parameters for the sources. The ratio of the NH$_3$ (2,2) and (1,1) measurements provides lower limits to the temperature of the cold, extended envelopes of each source. We use published data with similar resolution to supplement some of our (2,2) data with poor signal–to–noise (see column 7 of Table 3). Next, we use the formaldehyde data which provides sensitivity to the density and the presence of any warm gas. A comparison of many H$_2$CO line ratios using a Large Velocity Gradient model provides initial estimates for both density and temperature (Mangum & Wootten 1993). Using these initial estimates, we then employ a more robust microturbulent radiative transfer model (one in which the size scale of velocity turbulence is small when compared to the photon mean–free path) to iteratively calculate the line intensities of the lower opacity para–formaldehyde species and obtain the best fit temperature and density model which reproduces the observed brightness temperatures. In some regions, multiple layers must contribute to the observed spectrum.

In general, low excitation transitions of H$_2$CO (e.g. $J_{K_{-1}K_1} = 1_{01} \rightarrow 1_{00}$ are compared to estimate the temperature and density in the cold region. Alternatively, a relatively warmer region tends to produce emission from higher energy transitions (e.g. $J_{K_{-1}K_1} = 5_{05} \rightarrow 4_{04}$). For example, towards IRAS4A, Wootten et al. (2001) find both low excitation ($\int T_R^* dV[J_{K_{-1}K_1} = 1_{01} \rightarrow 1_{00}] = 4.21 \pm 0.09$ K km s$^{-1}$) and high excitation ($\int T_R^* dV[J_{K_{-1}K_1} = 5_{05} \rightarrow 4_{04}] = 3.63 \pm 0.15$ K km s$^{-1}$) lines of H$_2$CO, indicating that a layer of high density, warm gas coexists with colder, low density gas.

We use these values for n and T as input parameters into a microturbulent model for NH$_2$D and NH$_3$. The partition function is determined over all energy levels in order to eliminate errors due to high temperature approximations. With the size of the region set by our beam, we essentially have one free parameter, the column density, to predict the integrated intensities. We match the intensities and line profiles of all of the hyperfine components of NH$_2$D and NH$_3$ along with estimates of the optical depth from the following equation:

$$\frac{\text{T}_{\text{B}}(m)}{\text{T}_{\text{B}}(s)} = \frac{1 - exp[-\tau(m)]}{1 - exp[-a\tau(m)]} \tag{1}$$

to determine the best fit column density. In equation 1 $m$ and $s$ stand for main and satellite hyperfine lines, respectively; T$_B$ is the observed brightness temperature; $\tau$ is the optical depth; and $a$ is the ratio of the satellite to main hyperfine intensities. We list all results in Tables 3 and 5 for the deutero–ammonia and ammonia column densities. $5\sigma$ upper limits for the line intensities and column densities are listed in Table 4. In Tables 6 & 7 we list the ammonia fractionation for single–temperature and multiple–layer models, respectively.

The quality of our NH$_3$ data was not sufficient for reasonable comparison with our NH$_2$D in all cases. In general, not all of the hyperfine components were obtained in one spectrum because of hardware errors in the velocity offsets.

This required us to carefully compare all column density estimates based on only a subset of the ammonia hyperfine components, with data of similar spatial and spectral resolution found in the literature. We list all references for ammonia data in Table 5. In all cases we find good agreement between our own $NH_3$ column density estimates and those available in the literature. This lends confidence to our estimates of ammonia deuterium fractionation.

### 3.1.2. *Para–to–Ortho Ratio for* $NH_2D$.

In Table 8 we list the Ortho–to–Para ratio for the 86 and 110 GHz transitions of $NH_2D$ for eight sources. If one compares the statistical weights, the 110 GHz line strength is three times weaker than the 86 GHz transition. Different excitation conditions may vary this ratio slightly. Direct comparison of the integrated line strengths indicated that the ratio $\int T_R^* dv[86\ GHz]/\int T_R^* dv[110\ GHz]$ is consistent with 3 for all sources we observed in both lines. We also determine the column density of ortho–$NH_2D$ for comparison to para–$NH_2D$. Again, we find that the ratios of the column densities in the upper levels of both transitions are consistent with three.

### 3.2. *Self–absorption*

We find asymmetric spectral features indicative of an inwardly increasing temperature gradient in low–mass protostars in the 86 GHz NH2D transitions towards NGC 1333 IRAS4A, L1448C, S68 FIRS1, and possibly in NGC 1333 IRAS4C and S68N. Very high resolution profiles show similar spectral signatures in $H_2CO$, $N_2H^+$, $HCO^+$, and CS (Mardones et al. 1997; Gregersen et al. 1997). Line asymmetries or skewness were computed using the following dimensionless quantity:

$$Skewness = \Sigma T(V - V_{LSR})^3 \Delta V/(\Sigma T \Delta V) \times \quad (2)$$
$$= \left\{ (\Sigma T(V - V_{LSR})^2 \Delta V)/(\Sigma T \Delta V) \right\}^{-3/2}$$

Here, we take a weighted sum over each of the hyperfine components to obtain an average skew of the entire $NH_2D$ line profile. For a line that possesses most of its emission at velocities less than the source's systemic velocity ("blue-ward" asymmetric), the skewness is negative; it is positive for a similar "red-ward" asymmetry. We list our calculations for those sources with significantly asymmetric line profiles in Table 10. This method indicates that IRAS4A and L1448C possess the largest blue asymmetry. The $NH_2D$ spectra of IRAS4C and S68N show strong blue-ward behavior as well. The relative uncertainty in the S68 FIRS1 data makes quantifying an asymmetry difficult. No sources show significant ($\gtrsim 1\sigma$) red-ward asymmetries.

### 4. DEUTERIUM CHEMISTRY AND AMMONIA

Gas-phase synthesis of $NH_2D$ is strongly supported by observational evidence for $H_3^+$ (McCall et al. 1998; Geballe & Oka 1996) and $H_2D^+$ (Stark, et al. 1999) ion–molecule chemistry model predictions, and limits to desorption mechanisms in the molecular gas towards our observed sources. We discuss grain desorption mechanisms in §**??**. For clarity, we briefly discuss the general ion–molecule chemistry responsible for $NH_2D$ and $NH_3$ production. We use the detailed models of Roberts & Millar (2000) and Turner (2001) to compare our data to

in §**??**. We refer the reader to those sources for a more extensive discussion. Using the most current set of reaction rates from the UMIST database (Millar, Farquhar & Willacy 1997), Roberts & Millar (2000) determined the most important chains for the deuterium injection into the ammonia production process. The three general schemes considered in the literature are:

$$H_2 + N^+ \rightarrow NH^+ + H \quad (3)$$
$$H_2^+ + N \rightarrow NH^+ + H \quad (4)$$
$$H_3^+ + N \rightarrow NH_2^+ + H \quad (5)$$
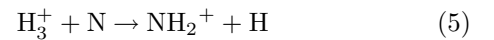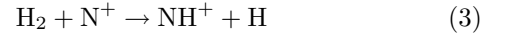
Reaction 3 is often rejected for $NH_3$ production because experiments performed at very low temperatures indicate a reaction endothermicity of 85K (Marquette et al. 1985) for thermal conditions. The corresponding reaction with HD, on the other had, has an endothermicity of 16K. This reaction also has the problem that $N^+$ is not very abundant. Herbst, Defrees, & McLean (1987) suggests that a nonthermal formation mechanism, where $N^+$ obtains additional translational energy in the reaction

$$N_2 + He^+ \rightarrow (N^+)^* + N + He \quad (6)$$
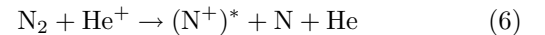
can provide the necessary abundance of $N^+$ for equation 3. A standard set of laboratory-determined reaction rates have not been determined. The range of rates lead to a factor of 10-100 variation in predicted ammonia abundances. Reaction 4 works well only for the formation of $NH_3$, since the deuterium equivalent has an energy barrier and limited abundance of $HD^+$. Reaction 5 has received much recent debate since its rate was remeasured by Scott et al. (1997) to be sufficient for ammonia (and, assuming the same rate, $NH_2D$) production. However, this contradicted earlier theoretical work which indicated that double–proton transfer was too inefficient (Huntress 1977), even if favored at cold temperatures. A more recent measurement for the rate of equation 5 indicates that the result of Scott et al. (1997) was erroneous. The authors no longer consider it a viable channel for ammonia production.

### 5. DISCUSSION

### 5.1. *Comparisons with gas–phase model predictions of* $NH_2D$.

We plot in Figure 7 the ammonia fractionation as a function of source temperature listed in Table 9. Observed values rise to ∼ 20 K; sources warmer than this have a flat $NH_2D/NH_3$ ratio. The range of $NH_2D/NH_3$ for massive hot cores is included as an arrow on the right side of the plot. We include curves (dashed–lines) based on the calculations of Roberts & Millar (2000) that bracket a range of values for $NH_2D/NH_3$. These model points are for steady–state models at densities of $10^4$ and $10^5 cm^{-3}$. The initial conditions of their models include a cosmic D/H and $HD/H_2$ ratio of $1.6 \times 10^{-5}$ (Linsky et al. 1995), a C/O ratio of 0.4, and a cosmic ray ionization rate of $1.3 \times 10^{-17} s^{-1}$. The range of model values plotted in Figure 7 includes a depletion of C, N, and O abundances by factors of 3 and 6. Larger depletions and densities lead to higher $NH_2D/NH_3$ values.

The observational result suggests that Class 0 and dark core sources have $NH_2D/NH_3$ values set by the earlier conditions of the parent cloud. Thus, we observe the "fossil remnants" of gas–phase chemistry when we study $NH_2D/NH_3$ towards these sources. The theoretical predictions of Roberts & Millar (2000), however, appear to conflict with the observed values, even for the coldest sources whose formaldehyde models consist of single, isothermal zones. The time–dependence of ammonia fractionation suggests a way to resolve this discrepancy. Roberts & Millar (2000) indicate that $NH_2D/NH_3$ values of $\sim 0.1$ are reached very quickly within a few $\times 10^3$ yrs, for isothermal 10 K sources at moderate densities of $10^4 cm^{-3}$ and persists for roughly $10^{5.5}$ yrs. In a pure gas–phase model, this decreases to $\sim 10^{-2}$ after $10^{5.5}$ yrs, while for a model that includes active grain accretion the fractionation rises above $10^{-1}$. This suggests that all of the sources except one (TMC1-CY) are at least $10^4$ yrs old. However, such age estimates are unconstrained. Additional deuterium fractionation ratios and abundances are necessary in order to fully test the validity of such a "chemical chronometer". One example that may help calibrate such a clock is recent modeling of CO depletion towards L1544 by (Caselli et al. 1999). Their dynamical and chemical modeling of CO, $H^{13}CO^+$, and $D^{13}CO^+$ line profiles suggests an age of at least $10^4$ years. They derive a $DCO^+/HCO^+$ ratio of $0.12 \pm 0.02$. We find $NH_2D/NH_3 = 0.13 \pm 0.02$ towards L1544 which, according to the model of Roberts & Millar (2000), is consistent with the age derived by (Caselli et al. 1999).

The two primary Taurus positions, TMC1-CY and TMC1-NH$_3$ offers a relative comparison of age estimates derived from deuterium fractionation ratios. Pratap et al. (1997) mapped the spatial distribution of 34 transitions of 14 molecules towards the Taurus Molecular Cloud ridge, which includes these sources. They argue that variations in the emission from carbon–bearing and other molecules result from both density and abundance variations. Pratap et al. (1997) find especially striking abundance gradients for SO, HC$_3$N, and CH$_3$CCH, which they explain with a small difference in the chemical evolution time-scale between the northeast and southwest ends of the cloud, or by a small change in the gas–phase C/O ratio. Both possibilities effectively reduce the carbon abundance, which would explain the lower abundances of cyanopolyynes in the northern regions near the ammonia peak. Comparisons of $NH_2D/NH_3$, $DCO^+/HCO^+$, DCN/HCN, and $N_2D^+/N_2H^+$ with the chemical model of Roberts & Millar (2000) satisfies both of these requirements. However, the age difference is preferred since both $NH_2D$ and $N_2H^+$ are considered to be largely derived from N$_2$. Molecular nitrogen is among the least reactive of neutral species in the ISM, making it likely to be abundant in the dense gas found in the more advanced stages of protostellar evolution.

Two recent studies of $NH_2D/NH_3$ by Tiné et al. (2000) and Saito et al. (2000) support and contradict, respectively, our conclusion that gas–phase chemistry is responsible for the ammonia deuterium ratios of L183 and TMC1-NH$_3$. Tiné et al. (2000) compare their observations with a simple–gas phase network based on the reaction rates of Millar et al. (1991). They successfully reproduce their observed abundances and deuterium fractionation ratios. Saito et al. (2000) on the other hand, compare $NH_2D$ data for several ammonia cores. They invoke grain synthesis of deuterated species even for their cold, star-less sources such as L183. Tiné et al. (2000) observed L134N ($1'$ NW of L183) and TMC1-N (equivalent to TMC1-NH$_3$). They experienced some ambiguity in modeling the spectra with an LVG code and relied instead on LTE values for determining $NH_2D$ column densities, analysis, and fractionation: $N(L134N) = 2 \times 10^{14}$ and $N(TMC1 - N) = 1.3 \times 10^{13}$; $X(L134N) = 1.5 \times 10^{-9}$ and $X(TMC1 - N) = 1.2 \times 10^{-10}$; (L134N) = 0.18 and $(TMC1 - N) = 0.02$.

We find $N(NH_2D)$ equal to $3 \times 10^{13}$ and $1 \times 10^{13}$ cm$^{-2}$, one and zero orders of mag different for L183 and TMC1-NH$_3$. However, we have beam dilution between effects between our 12 m observations and the 30 m survey of Tiné et al. (2000) and different positions, for L183. Our abundances, columns and fractionations for TMC1-NH$_3$ are fairly similar. Tiné et al. (2000) are able to reproduce their observations with extensive gas–phase modeling of the ammonia chemistry, with a few important caveats. Moderate to significant (factors of a few to 10) depletion of carbon and oxygen (i.e. removal of neutral and atomic destroyers, and reduction of $X_{e-}$) will help achieve the high abundances and fractionations (0.02 and 0.1 for L134N and TMC1–N, respectively). Our results for TMC1-NH$_3$ and L183 are similar, though we find a factor of two smaller deuterium fractionation towards L183. Additionally, we have been able to extend our analysis to other dark cores, which also indicates that gas–phase chemistry is most important. This suggests that grain processes are unimportant for these low mass cores, at least for ammonia formation and deuterium fractionation.

The results of Saito et al. (2000) are discrepant with our view that gas–phase synthesis dominates the formation of $NH_2D$. They studied $NH_2D/NH_3$ for 16 ammonia cores from the Benson & Myers (1983) list and found that mostly those with *IRAS* detections show elevated or observable $NH_2D$ abundances and $NH_3$ fractionation. Furthermore, they find larger abundances than expected from gas–phase networks for the kinetic temperatures of 4 sources. They concluded that ammonia is formed and deuterated on grains. Several problems exist with their analysis. First, a notable exception to their conclusions regarding grain–chemistry formation of $NH_2D$ is L183, where they find abundances and fractionations similar to our own. Second, they use an LTE estimate of the excitation of $NH_2D$, which tends to over-predict the column density. This is because in an LTE scenario, one requires a larger abundance (column density or optical depth of $NH_2D$) to achieve the same line intensities than for non-LTE methods. Third and last, they did not integrate enough on all of their sources, since TMC1-NH$_3$ has a clear detection by us and by Tiné et al. (2000). Thus, it is also possible that for their dark cores without infrared sources, the column density of $NH_2D$ may be below the detection limit of their survey.

Observational and theoretical comparison of L183 and TMC1-NH$_3$ provide important benchmarks for gas–phase synthesis of molecules (Swade 1987). L183 and TMC1–NH$_3$ possess similar values of $n$, $T$, and size, but dis-

play very different chemical characteristics. Most chemical and dynamical models of L183 have concentrated on the dearth of cyanopolyynes and abundance of sulferetted molecules. Deuterium fraction may provide additional constraints. Ammonia fractionation is larger by a factor of two in L183 when compared to TMC1–NH$_3$. Different initial abundances between L183 and TMC1 have generally been ruled out by their relative isolation and similar galactocentric distance. TMC1–NH$_3$ should, as a whole, be older than L183 based on time–evolution models of hydrocarbons; however the same cannot be said for sulphur, which is observed to have lower abundances in TMC1 resulting in the conclusion that L183 is older. Swade (1987) points out that the conflicting chemical histories of L183 and TMC1–NH$_3$ can be rectified in terms of larger depletions in TMC1. In order to achieve this, one requires a larger molecular hydrogen *volume* density, which in cold gas leads to more easily depleted material. The slightly lower abundance of ammonia (which we observe) is consistent with a larger depletion in TMC1–NH$_3$.

## 5.2. *Sources with warm gas and more complex structure*

Our H$_2$CO modeling indicates that several sources (L1448IRS3, NGC 1333 IRAS4A, NGC 1333 IRAS2, NGC 1333 IRAS7, S68 FIRS1, and S68N) are well fitted with two distinct layers with different densities and temperatures. We do not know for a certainty where all of the NH$_2$D and NH$_3$ is located. The reason for this discrepancy is the inherent ambiguity in our source models. We are able to arbitrarily place the ammonia in either the warm or cold zones, and still successfully reproduce the observed integrated intensity. Therefore, we know only what the *total* column density and column density ratios are towards these sources. The lack of knowledge about the grain contributions to the observed deuterium fractionation makes an accurate census difficult. However, similarity between column density ratios among Tables 6 (cold, single layer) and 7 (warm, multi-layer) does not suggest an extra warm gas contribution is necessary. Those profiles that show well–resolved self–reversal provide a tool to break this degeneracy. We concentrate on IRAS4A, since it contains the most well resolved line profiles, and is thus easiest to consider. Higher spectral resolution data are necessary for a less ambiguous estimate of the column density distribution in the other self–absorbed sources.

### 5.2.1. *Foreground Absorption in IRAS4A*

An extended, cool envelope may explain the self–absorbed profile observed towards IRAS4A. We estimate a *lower* limit to the self-absorbing layer of NGC 1333 IRAS4A. We assume that the NH$_2$D absorbing layer is primarily cold gas near 25K located along the line–of–sight in the central 0.5 km s$^{-1}$. We estimate the lower limit to the absorbing layer column density by assuming that the optical depth is 1 and varying the temperature. We find that the column density must be at least a few times $10^{13}$ cm$^{-2}$ for temperatures between 10 and 25 K (the temperature of the cold layer in our micro-turbulent model).

This allows us to fix the column density in the outer layers of IRAS4 to *at least* $1 \times 10^{13}$ cm$^{-2}$ and estimate the total column density with our micro-turbulent model

by fitting the observed integrated intensity listed in Table 3. Using this as an initial guess we estimate the column density towards IRAS4A in the warm gas is at least a factor of 10 less than in the colder gas. The ammonia data lacks the spectral resolution to permit a similar analysis. If we arbitrarily divide the NH$_3$ column density evenly between the warm and cool layers (*i.e.* assume that NH$_3$ itself is ubiquitous and well–mixed in the ISM), NH$_2$D/NH$_3$ falls off by about a factor of 10. This is roughly the expectation from *gas–phase* chemical models of deuterium fractionation. However, in addition to the lack of spectral resolution in the NH$_3$ data, we are not resolving any spatial structure towards IRAS4A. High spatial resolution analysis are necessary to understand the distributions of NH$_2$D and NH$_3$.

## 5.3. *Grain Deuteration*

Grain enhancements may provide an important alternative source for deuterium fractionation of ammonia for Class 0 sources. Though we suggest that the flat trend in NH$_2$D/NH$_3$ for sources warmer than 20 K indicates a gas–phase origin, it is important to discuss the general scheme here. Grain accretion time scales in dense cores are of order the collapse time scale, $\lesssim 10^6$yrs. The larger mass of deuterium allows it to stick longer to a surface, and bind more strongly than hydrogen with other atoms. Observations of D$_2$CO/H$_2$CO (Turner 1990; Castets et al. 1999), HDO/H$_2$O (Jacq et al. 1990), and CH$_3$OD/CH$_3$OH (Mauersberger et al. 1988), underscore the importance of grain–based molecular formation and fractionation, although more recent gas–phase synthesis models (e.g. Roberts & Millar 2000) suggest otherwise.

A grain origin for NH$_2$D is suggested based on the similarity of the fractional abundances of NH$_2$D in TMC1 versus the Orion Hot Core. A review of the abundances using standard methods is appropriate at this point. Walmsley et al. (1987) find that the NH$_2$D emission is optically thin in the Orion–KL region. They obtain N(NH$_2$D)=$1.54 \pm 0.4 \times 10^{14}$. Using the dust continuum measurements of Masson et al. (1985) to estimate the NH$_2$D fractional abundance, one finds $X[\text{NH}_2\text{D}]=1.01 - 6.21 \times 10^{-10}$. Using the C$^{18}$O value from Ungerechts et al. (1997) and the conversion factor for carbon monoxide to molecular hydrogen developed by Frerking, Langer & Wilson (1982), N(H$_2$) is a factor of 10 smaller than the dust value. Therefore, the abundance of deuterated ammonia is equivalently larger by ten. Towards TMC1, only C$^{18}$O data is available, and we find NH$_2$D/H$_2$ = $4.91 \pm 1.63 \times 10^{-10}$, quite similar to the Orion Hot Core. Abundance comparisons, in general, are problematic, especially between physically different regions such as TMC1 and the hot core associated with IRc2. CO to molecular hydrogen conversion factors and line-of-sight complexity towards a source are difficult to properly estimate. Therefore, abundance studies should be approached with some caution[3].

An important distinction between our source list and hot cores used in studies such as Walmsley et al. (1987) and Jacq et al. (1990) is the temperature. Desorption mechanisms will be largely ineffective at removing any depleted or surface-chemistry products in dark clouds, unless

---

[3] See the discussion by Mundy & McMullin (1996).

low-temperature, non-thermal desorption such as $H_2$ formation on grains (which releases $\sim 4.5$ eV of energy) occurs rapidly. This will only occur for low density regions, where $H_2$ formation theoretically prevents the condensation of CO and water on small grains and PAHs (Duley & Williams 1993). Even for the more evolved Class 0 objects included here, grain chemistry can be excluded because of the sublimation temperature of ices. Grain mantles are dominated by water ice (e.g. Ehrenfreund & Charnley 2000), whose sublimation temperature is 90K. Since our sources are all cooler than this, grain sublimation is not likely. In fact, thermal grain desorption at low temperatures and densities above $10^5$ cm$^{-3}$ proves quite inefficient, even in the most optimistic models where tunneling on small grains occurs, reaction exothermicities exceed binding energies, and $H/H_2$ is large enough to quickly saturate C, O, and N atoms. We discuss several other grain desorption mechanisms below, under the assumption that surface deuterium enhancements may contribute to the observed $NH_2D/NH_3$. These include: thermal, cosmic-ray induced grain heating, photo-desorption, collisional (grain-on-grain violence). Impulse heating of grains (temporarily increasing the temperature of a single grain above the threshold for thermal desorption) is achieved with X-rays and cosmic rays. Léger et al. (1985) investigated this affect in regions of varying density and visual extinction. For $n < 10^4$ cm$^{-3}$ and $A_V < 5$, desorption efficiently removes CO and even water–ammonia ice mantles quite readily. However, for more dense regions, the water-ammonia lattice will remain, since for $A_V \gtrsim$ few UV photons cannot penetrate them. Wootten, Loren, & Snell (1982); Butner, Lada, & Loren (1995); Williams et al. (1998) have shown that X–ray contributions appear to be minimal since the electron fraction measured via $DCO^+/HCO^+$ varies little for sources with and without stars. Therefore, our sources would have little cosmic–ray desorbed input from abundances of ammonia either stored or produced on grains.

## 6. CONCLUSIONS

We observed $NH_2D$ hyperfine transitions towards 32 protostellar and pre–stellar sources with similar spatial resolution. We find nearly a 70% detection rate for the $NH_2D$ lines at 85.9 GHz. The observed abundances of $NH_2D$ when compared to single–dish $NH_3$ observations of similar beam–width, indicate that the deuterium fractionation is large, $10^{-3} \lesssim NH_2D/NH_3 \lesssim 10^{-1}$. The observed $NH_2D/NH_3$ values generally exceed or equal those seen in hot core regions as well as in warm, embedded condensations in otherwise low luminosity sources with large, cold envelopes. Sources with $T_K \lesssim 20$ K follow gas–phase predictions for $NH_2D/NH_3$; for $T_K > 20$ K the trend flattens, indicating that Class 0 sources have not begun to destroy $NH_2D$. $NH_2D/NH_3$ ratios reflect the "fossil" remnants of gas–phase synthesis. We additionally conclude that grain formation of deuterated ammonia is not necessary to explain $NH_2D/NH_3$.

Some evidence exists that dynamical ages of protostellar sources can be derived from comparisons of deuterium fractionation and chemical models of star forming cores. However, this notion is currently rather speculative. We are able to address *relative* evolutionary differences between sources such as TMC1-CY, TMC1-NH$_3$, and L183 successfully.

Self–reversed profiles indicate that the overall story for $NH_2D$ is far more complicated, however. Indeed, future careful modeling and observations will attempt to address the coupled influences of chemistry and dynamical evolution in IRAS4. Nonetheless, $NH_2D$ provides important insights into deuteration in the ISM. Deuterium fractionation not only varies among sources of different physical attributes, but also among different molecules. Thus, a full census of deuterium fractionation seems necessary in order to test astrochemical models. Furthermore, with deuterated molecules now providing information on the collapse regions of protostars, new and potentially powerful tools for examining the history of core collapse via chemical evolution models can provide checks on more traditional methods.

## REFERENCES

André P., Ward-Thompson, D., Barsony, M. 1993, ApJ, 406, 122.
Bachiller, R., Guillateau, S., Kahane, C. 1987, A&A, 173, 324.
Bachiller, R., Martin–Pintado, J. Planesas, P. 1991, A&A, 251, 639.
Bates, D.R. 1986a, ApJ, 306, L45.
Bates, D.R. 1987a, in *Modern Applications of Atomic & Molecular Physics*, ed. A.E. Kingston (London:Plenum), p. 41.
Bates, D.R. & Herbst, E. 1988, in *Rate Coefficients in Astrochemistry*, ed. T.J. Millar & D.A.Williams (Dordrecht:Kluwer), p.41.
Batrla, W., Wilson, T.L., Bastien, P., & Ruf, K. 1983, A&A, 128, 279
Benson, P.J. & Myers, P.C. 1983, ApJ, 266, 309.
Bergin, E.A. & Langer, W.D. 1997, ApJ, 486, 316.
Bester, M., Urban, S., Yamada, K., & Winnewisser, G. 1983, A&A, 121, L13.
Blake, G.A., Sandell, G. , van Dishoeck, E.F., Groesbeck, T.D., Mundy, L.G. & Aspin, C. 1995, ApJ, 441, 689.
Brown, P.D., Millar, T.J. 1989, MNRAS, 237, 661 (1989a).
Brown, P.D., Millar, T.J. 1989, MNRAS, 240, 25P (1989b).
Brown, P.D., Charnley, S.D., & Millar, T.J. 1988, MNRAS, 231, 409.
Butner, H., Lada, E., Loren, R. 1995, ApJ, 448, 207.

Caselli, P., Walmsley, C.M., Tafalla, M., Dore, L., & Myers, P.C. 1999, ApJ, 523, L165
Castets, A., Ceccareli, C., Loinard, L., Caux, E., Tielens, A.G.G.M. "The Physics & Chemistry of the Interstellar Medium, Proceedings of the 3rd Cologne-Zermatt Symposium," 1998, eds. V. Ossenkopf, J. Stutzki, & G. Winnewisser, GCA-Verlag Herdecke.
Cesaroni, R., Wilson, T.L. 1994, A&A, 281, 209.
Charnley, S.B., Tielens, A.G.G.M. & Millar, T.J. 1992, ApJ, 399, L71.
Dalgarno, A. & Lepp, S. 1984, ApJ, 287, L47.
Danby,G., Flower, D.R., Valiron, P., Schilke, P., Walmsley, C.M. 1988, MNRAS, 235, 229.
Dinger, A.S.C. & Dickinson, D.F. 1980, AJ, 85, 1247.
Draine, B.T. & McKee, C.F. 1993, ARA&A, 31, 373.
Duley, W. W. & Williams, D. A. 1993, MNRAS, 260, 37.
Ehrenfreund, P. & Charnley, S.B. 2000, ARA&A, 38, 427
Eiroa, C. & Casali, M.M. 1989, A&A, 223, L17.
Frerking, M.A., Langer, W.D. & Wilson, R.W. 1982, ApJ, 262, 590.
Geballe, T. R. & Oka, T. 1996, Nature, 384, 334.
Gellene, G.I. & Porter, R.F. 1983, *Accounts Chem. Res.*, 16, 200.
Gellene, G.I. & Porter, R.F. 1984, J. Chem. Phys., 88, 6680.

Greason, M.R. 1986, Master's Thesis, Chemical trace of HCN using DCN, University of Virginia.

Gregersen, E., Evans, N., Zhou, S., & Choi, M. 1997, ApJ, 484, 256.

Herbst, E., Defrees, D.J., & McLean, A.D., 1987, ApJ, 321, 898.

Ho, P.T.P. & Barrett, A.H. 1980, ApJ, 237, 38.

Ho, P.T.P., Townes, C.H. 1983, ARA&A, 21, 239.

Hollenbach, D. 1997, IAU Symp. 182: *Herbig-Haro Flows and the Birth of Stars*, 182, 181.

Huntress, W.T. 1977, ApJS, 33, 445.

Jacq, T., Walmsley, C.M., Henkel, C., Baudry, A., Mauersberger, R., & Jewell, P.R. 1990, A&A, 228,447.

K., Kaifu, N. Ohishi, M., Takano, S. Ishikawa, S. Masuda, A. 1992, ApJ, 394, 539.

Léger, A., Jura, M., & Omont, A. 1985, *A&A*, 144, 147.

Lepp, S. & Dalgarno, A. 1988, ApJ, 324, 553.

Linsky, J.L., Diplas, A., Wood, B.E., Brown, A., Ayres, T.R. &Savage, B.D. 1995, ApJ, 451, 335.

Loren, R.B. & Wootten H.A. 1985, ApJ, 299, 947.

Loren, R.B., Evans, N.J., II & Knapp, G.R. 1979, ApJ, 234, 932.

Mangum J.G. & Wootten A. 1993, ApJS, 89, 123.

Mangum, J.G., Wootten, A., & Mundy, L. 1992, ApJ, 388, 467.

Mangum J.G., Wooten A., Wadiak E.J. & Loren R.B. 1990, ApJ, 348, 542.

Mardones D., Myers, P.C., Tafalla, M., & Wilner, D.J. 1997, ApJ, 489, 719.

Masson C.R., Claussen M.J., Lo K.Y., Moffet A.T., Phillips T.G., Sargent A.I., Scott S.L. & Scoville N.Z. 1985 ApJ, 295, L47.

Marquette, J.B., Rowe, B.R., Dupeyrat, G., & Roueff, E. 1985, A&A, 147, 115.

Martin-Pintado, J. & Cernicharo, J. 1987, A&A, 176, L27

Martin-Pintado, J., Wilson, T. L., Gardner, F. F. & Henkel, C. 1983, A&A, 117, 145.

Mauersberger, R., Henkel, C., Jacq, T., & Walmsley, C. M. 1988, A&A, 194, L1.

McCall, B.J., Hinkle, K.H., Geballe, T.R., & Oka, T. 1998, Faraday Discuss., 109, 267.

Millar, T.J., Farquhar, P.R.A. & Willacy, K. 1997, A&AS, 121, 139.

Millar,T.J., Bennett,A., Rawlings,J.M.C.,Brown,P.D.,Charnley,S.B. 1991, *Astr.Apj.Suppl.* 1991, 87, 585.

Millar, T.J., Bennet, A., Herbst, E. 1989, ApJ, 340, 906.

Mundy, L.G. & McMullin, J.P. 1996, IAU Symp. 178: *Molecules in Astrophysics: Probes & Processes*, 178, 183.

Olberg, M., Bester, M., Rau, G., Pauls, T., Winnewisser, G., Johansson, L. E. & Hjalmarson, A. 1985, A&A, 142, L1.

O'Linger,J., Wolf-Chase,G., Barsony,M., Ward-Thompson,D. 1999, ApJ, 515, 696.

Pagani, L.P. & Nguyen–Q–Rien 1987, A&A, 181, 112.

Peng, Y. Vogel, S. N., & Carlstrom, J. E. 1993, ApJ, 418, 255.

Penzias, A. A. 1979, ApJ, 228, 430.

Pickett, H.M., Poynter, R. L., Cohen, E. A., Delitsky, M. L., Pearson, J. C., & Muller, H. S. P. 1998, *J. Quant. Spectrosc. & Rad. Transfer*, 60, 883.

Pratap,P., Dickens,J.E., Snell, R. L., Miralles,M.P.,Bergin,E.A., Irvine, W.M., Schloerb,F.P. 1997, ApJ, 486, 862.

Rawlings, J.M.C., Hartquist, T.W., Menten, K.M. & Williams, D.A. 1992, MNRAS, 255, 471.

Roberts, H., Millar, T.J., 2001, A&A, 361,388.

Rodriguez, L.F., Moran, J.M., Gottlieb, E.W. & Ho, P.T.P. 1980, ApJ, 235, 845.

Rodriguez, L.F., Curiel, S., Moran, J.M., Mirabel, I.F., Roth, M. & Garay, G. 1989, ApJ, 346, L85.

Rodriguez, L.F., Escalante, V., Lizano, S., Canto, J., Mirabel, I.F. 1990, ApJ, 365, 261.

Rodriguez–Kuiper, E.N., Kuiper, T.B.H., Zuckerman, B., 1978, ApJ, 219, L49.

Roueff, E., Tiné, S., Coudert, L. H., Pineau des Forêts, G., Falgarone, E. and Gerin, M. 2000, A&A, 354, L63.

Saito, S., Ozeki, H., Ohishi, M., Yamamotot, S. 2000, ApJ, 535, 227. bibitem[Scott et al.(1998)]scott1998Scott, G.B.I., Freeman, C.G., McEwan, M.J. 1998, J. Chem. Phys., 109, 9010.

Scott, G.B.I., Freeman, C.G., McEwan, M.J. 1997, MNRAS, 290, 636.

Shah, R. Y., Wootten, H. A., & Mangum, J. BAAS, 1997, 191.2001.

Shah, R.Y., & Wootten, A. 1999, IAU 192: *Astrochemistry: from Molecular Clouds to Planetary Systems*, in press.

Stark, R. , van der Tak, F.F.S. & van Dishoeck, E.F. 1999, ApJ, 521, L67 .

Stutzki, J. Winnewisser, G. 1985, A&A, 148, 254.

Swade, D.A. 1987, Ph.D. Thesis.

Tielens A.G.G.M. 1983, A&A, 119, 177.

Tiné, S., Roueff, E., Falgarone, E., Gerin, M. and Pineau des Forêts, G. 2000, A&A, 356, 1039.

Townes, C.H., Schawlow, A.L. 1955, Microwave Spectroscopy (New York: Dover).

Turner, B. E. 2000, in preparation.

Turner, B. E. 1990, ApJ, 362, L29

Turner, B.E., Zuckerman, B., Morris, M., & Palmer, P. 1978, ApJ, 219, 43.

Ungerechts, H. , Bergin, E.A., Goldsmith, P.F., Irvine, W.M., Schloerb, F.P. & Snell, R.L. 1997, ApJ, 482, 245.

Ungerechts, H. & Guesten, R. 1984, A&A, 131, 177.

van Dishoeck, E.F. & Blake, G.A. 1998, ARA&A, 36, 317.

Walker, C., Narayan, G., & Boss, A. 1994, Astrophysical. J., 431, 767.

Walmsley, C.M., Hermsen, W., Henkel, C., Mauersberger, R., & Wilson, T.L. 1987, A&A, 172, 311.

Watson, W.D. 1974, ApJ, 188, 35.

Williams, J.P., Bergin, E.A., Caselli, P., Myers, P.C., & Plume, R. 1998, ApJ, 503.

Wootten,A., &ré,P., Despois,D., Sargent,A. 2001, private communication.

Wootten, H.A, Loren, R.B. 1987, ApJ, 317, 220.

Wootten, H.A. 1987, IAU, 140.

Wootten, A., Loren, R. B., Snell, R. L. 1982, ApJ, 255, 160.

Wootten, H.A., Mangum, J.G. 1993 BAAS, 183, 49.03.

Zeng, Q., Batrla, W. & Wilson, T. L. 1984, A&A, 141, 127.
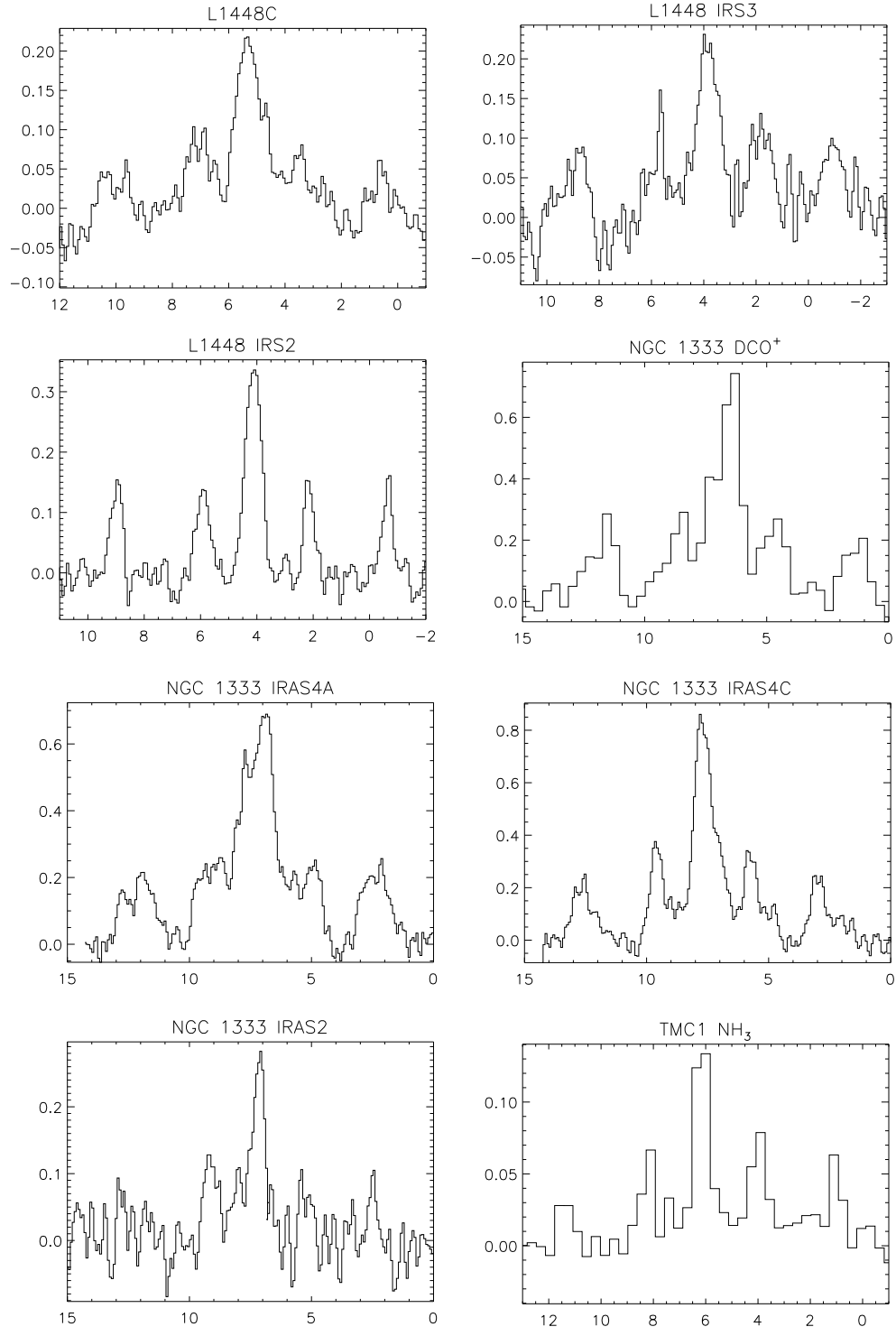
FIG. 1.— 85.9 GHz $NH_2D$ spectra. The spectral resolution is 0.13 km s$^{-1}$/channel except for NGC1333 DCO$^+$ and TMC1 $NH_3$ where it is 0.35 km/s. A linear baseline is removed from the data, revealing the hyperfine components.
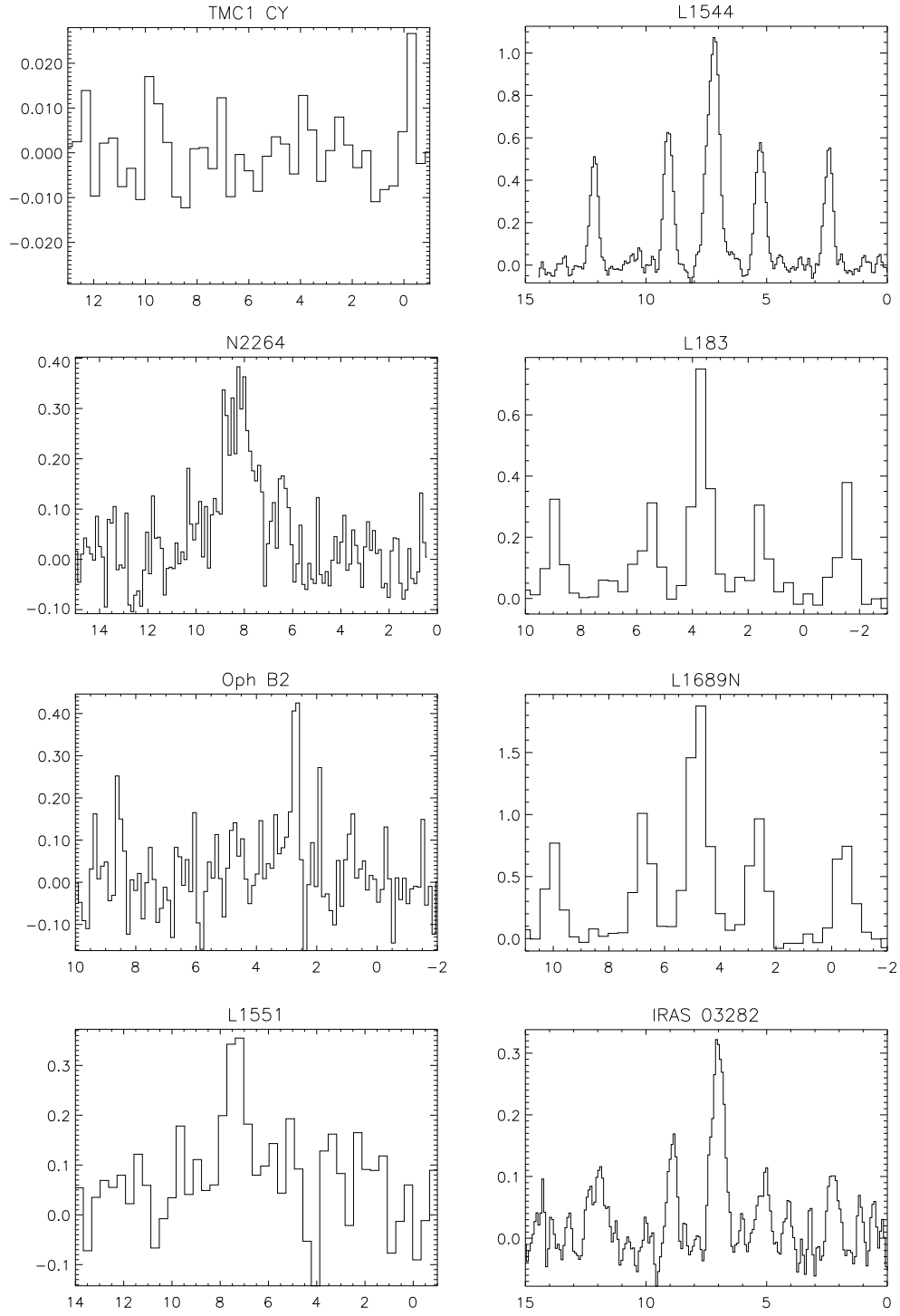
F<small>IG</small>. 2.— Same as figure 1. Here TMC1 CY, L183, L1689N and L1551 are observed with the coarser 0.35 km/s resolution.
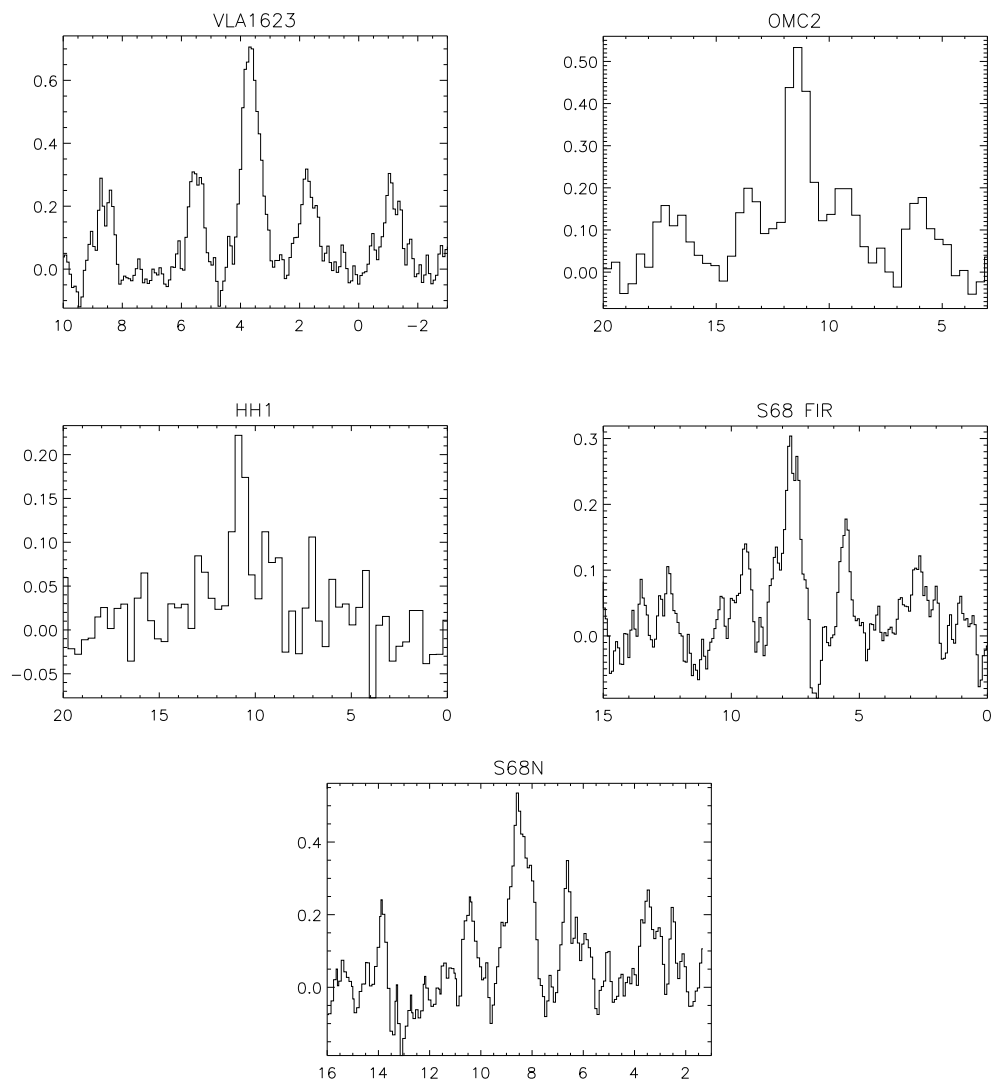
FIG. 3.— Same as figure 1. Here TMC1 CY, L183, L1689N and L1551 are observed with the coarser 0.35 km/s resolution.

12
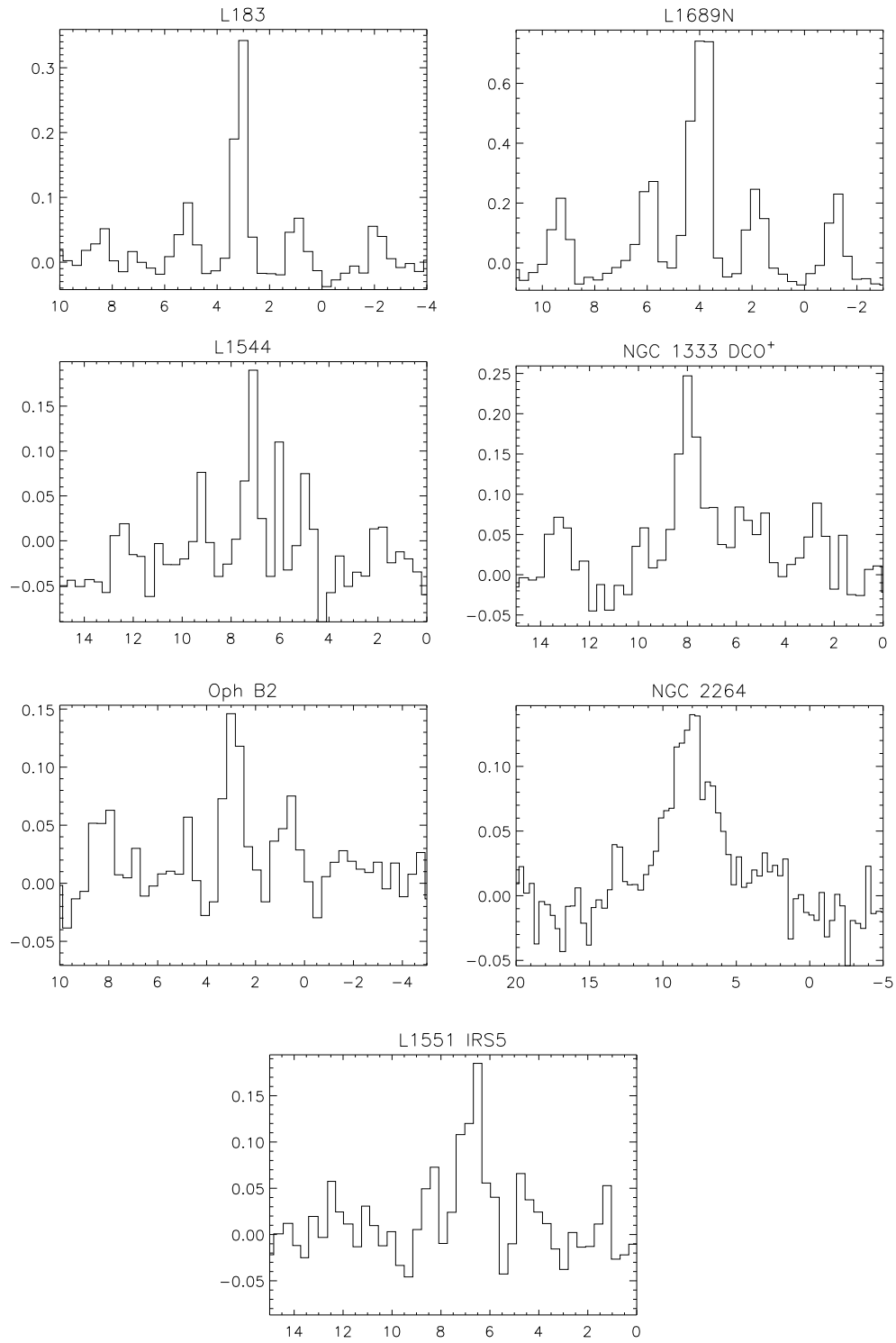


FIG. 4.— 110.1 GHz NH$_2$D spectra. The spectral resolution is 0.35 km s$^{-1}$/channel. A linear baseline is removed from the data, revealing the hyperfine components.
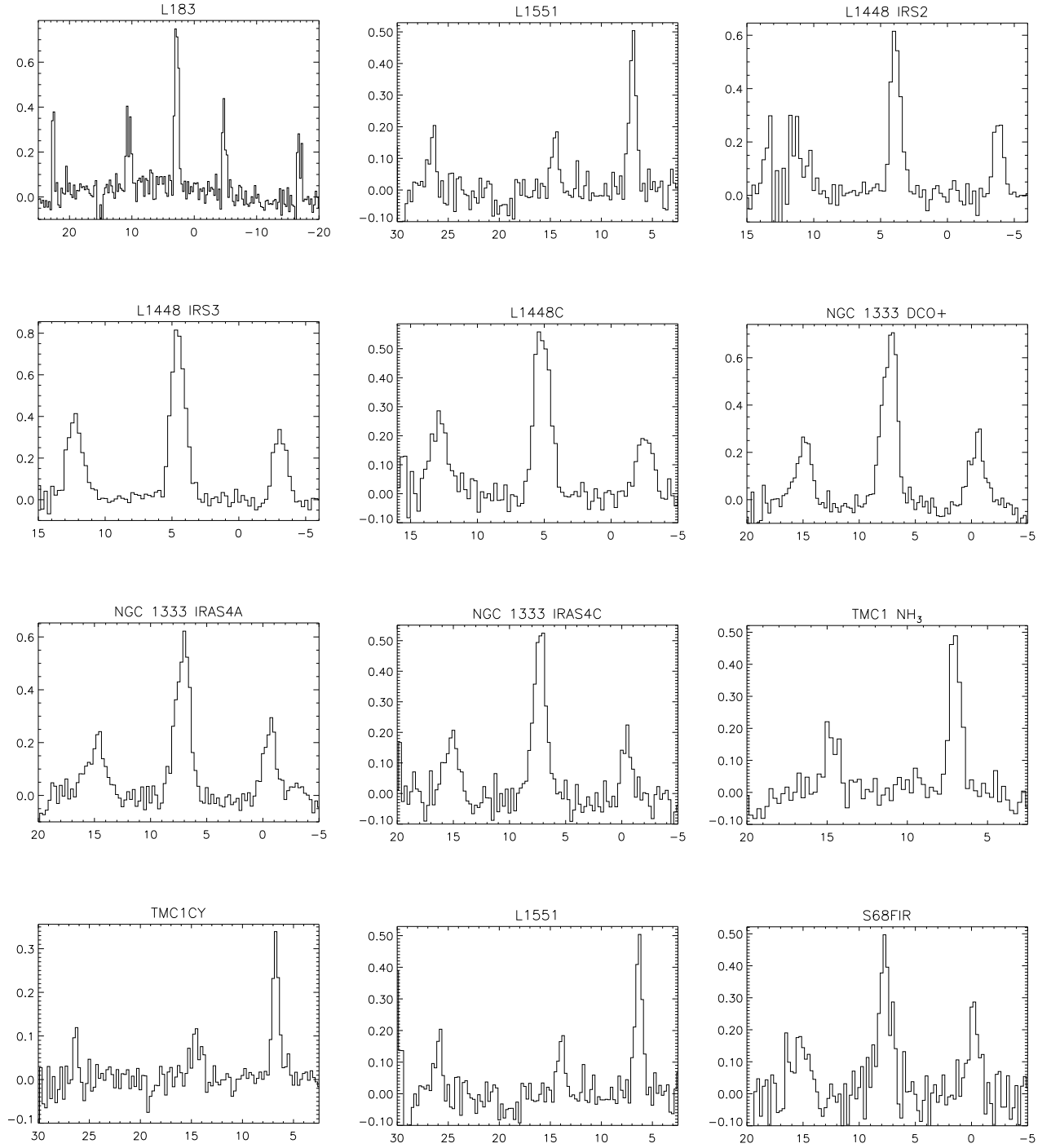
FIG. 5.— 23.6 GHz NH$_3$ spectra. The spectral resolution is 0.25 km s$^{-1}$/channel. A linear baseline is removed from the data, revealing the hyperfine components.
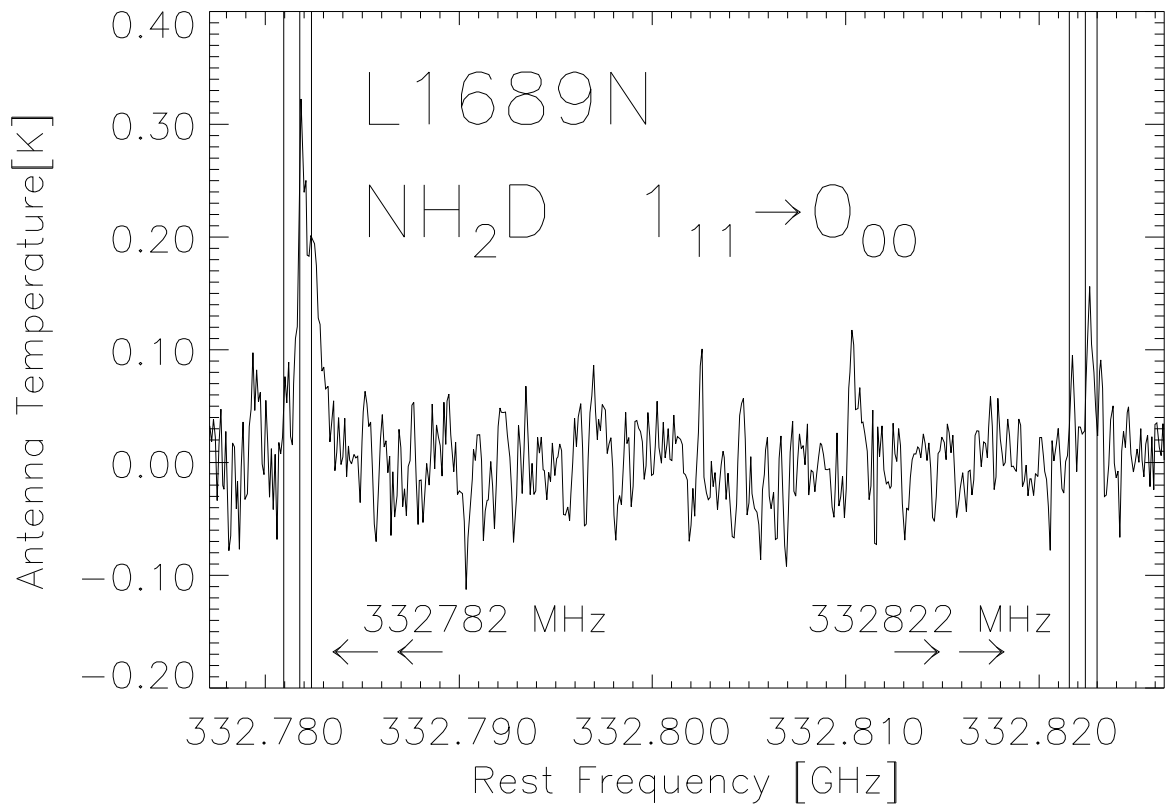
FIG. 6.— Plot of the 333 GHz $J = 1_{11} \rightarrow 0_{00}$ fundamental transition NH$_2$D observed with the Caltech Submillimeter Observatory. The spectral resolution is 0.04 km s$^{-1}$ for this 1.5 hour spectrum. Both sets of lines near 332.820 and 332.782 GHz are heavily blended. The integrated intensity is consistent with an LTE distribution.
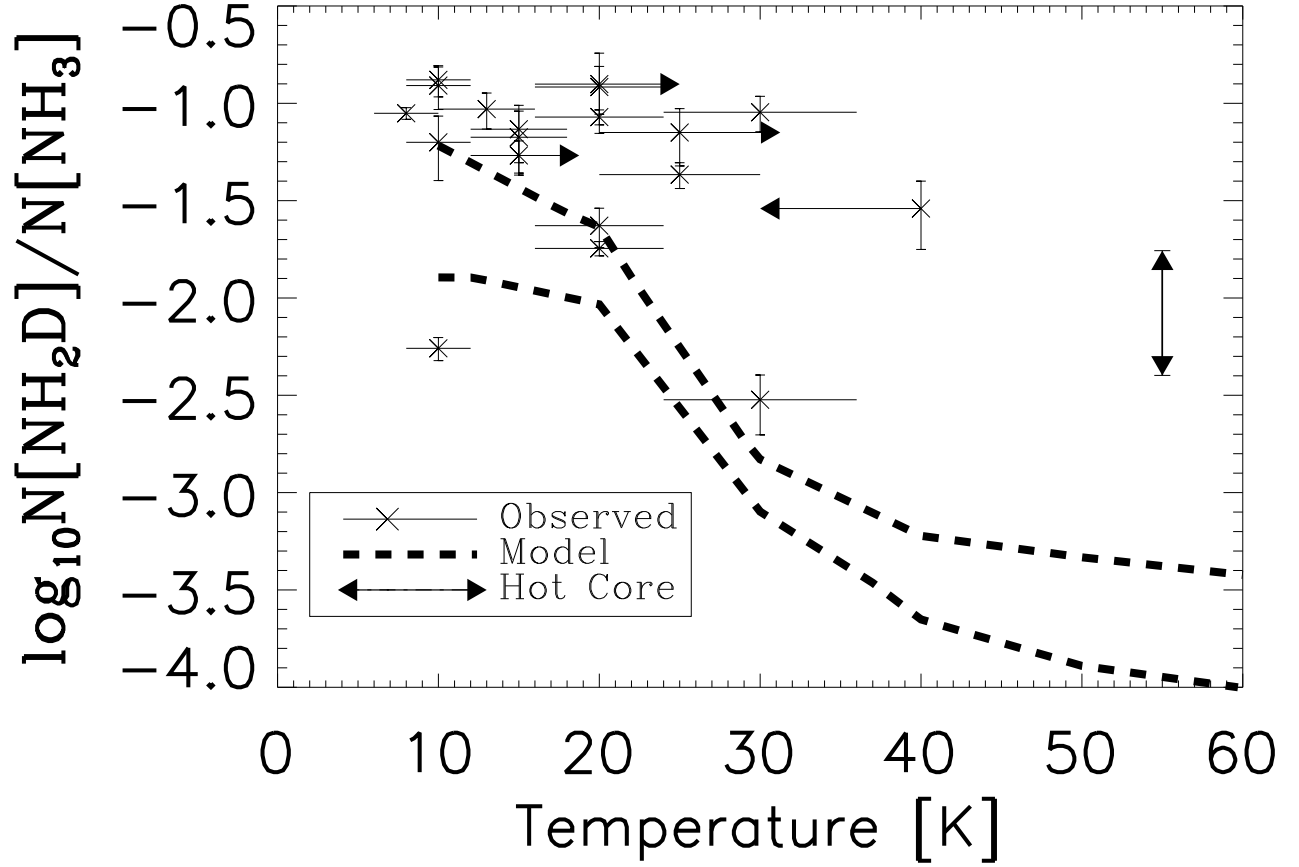
FIG. 7.— Plot of ammonia fractionation versus temperature for sources with single temperature H₂CO models (crosses). We include the predicted ammonia fractionation from the steady–state gas phase models of Roberts & Miller (2000) as upper and lower ranges marked with dashed lines. Additionally, we plot the range of values found for hot cores by various authors (*N.B.* the temperature choice is arbitrary)

TABLE 1
DEUTERO–AMMONIA TRANSITION FREQUENCIES

| Transition | $F' - F''$ | Intensity | Frequency (GHz)[†] |
|---|---|---|---|
| | 0–1 | 0.111 | 85.9247829 |
| | 2–1 | 0.139 | 85.9257031 |
| $J = 1_{11} \to 1_{01}$ | 2–2 | 0.417 | 85.9262703 |
| $J = 1_{11} \to 1_{01}$ | 1–1 | 0.083 | 85.9263165 |
| | 1–2 | 0.139 | 85.9268837 |
| | 1–0 | 0.111 | 85.9277345 |
| | 0–1 | 0.111 | 332.7809447 |
| $J = 1_{01} \to 0_{00}$ | 2–1 | 0.556 | 332.7817955 |
| | 1–1 | 0.333 | 332.7823627 |
| | 0–1 | 0.111 | 110.152084 |
| | 2–1 | 0.139 | 110.152995 |
| $J = 1_{11} \to 1_{01}$ | 2–2 | 0.417 | 110.153599 |
| $J = 1_{11} \to 1_{01}$ | 1–1 | 0.083 | 110.153599 |
| | 1–2 | 0.139 | 110.154222 |
| | 1–0 | 0.111 | 110.155053 |
| | 0–1 | 0.111 | 332.8215595 |
| $J = 1_{01} \to 0_{00}$ | 2–1 | 0.556 | 332.8224149 |
| | 1–1 | 0.333 | 332.8229853 |

[†]Tiné et al. 2000; Townes & Schawlow 1955

TABLE 2
SOURCE LIST

| Source | R. A. (1950) h  m  s | DEC (1950) ° ′ ″ | $V_{LSR}$ km s$^{-1}$ |
|---|---|---|---|
| L1448 IRS2 | 03 22 17.9 | 30 34 41 | 4.0 |
| L1448 NW | 03 22 31.1 | 30 35 14 | 5.4 |
| L1448 IRS3 | 03 22 31.9 | 30 34 45 | 4.7 |
| L1448 C | 03 22 34.4 | 30 33 35 | 5.4 |
| NGC 1333 DCO$^+$ | 03 26 3.60 | 31 04 42 | 7.0 |
| NGC 1333 IRAS7 | 03 26 6.90 | 31 08 28 | 7.0 |
| NGC 1333 IRAS2 | 03 25 52.6 | 31 04 30 | 7.0 |
| NGC 1333 IRAS4A | 03 26 4.78 | 31 03 14 | 7.0 |
| NGC 1333 IRAS4B | 03 26 7.00 | 31 02 52 | 7.0 |
| NGC 1333 IRAS4C | 03 26 8.10 | 31 03 37 | 7.0 |
| IRAS 03282 | 03 28 15.2 | 30 35 14 | 7.0 |
| IRAS 03367–IC 348 | 03 36 47.1 | 31 47 29 | 7.0 |
| L1551 | 04 28 40.2 | 18 01 42 | 6.5 |
| TMC1 AM | 04 38 19.5 | 25 42 29 | 6.0 |
| TMC1 CY | 04 38 38.0 | 25 35 45 | 6.0 |
| L1512 | 05 00 54.5 | 32 40 00 | 7.9 |
| L1544 | 05 01 15.0 | 25 07 00 | 7.1 |
| OMC2 | 05 32 58.0 | -05 12 11 | 11.0 |
| HH1 | 05 33 52.0 | -06 47 09 | 10.0 |
| NGC 2264 | 06 38 24.9 | 09 32 29 | 8.0 |
| L183 | 15 51 30.0 | -02 43 31 | 3.0 |
| VLA1623 | 16 23 25.0 | -24 17 47 | 4.0 |
| OPHB1 | 16 24 09.0 | -24 22 49 | 3.0 |
| OPHB2 | 16 24 26.3 | -24 19 49 | 3.0 |
| IRAS 16293 | 16 29 21.0 | -24 22 16 | 4.1 |
| L1689N | 16 29 27.6 | -24 22 08 | 4.0 |
| L63 | 16 47 17.0 | -18 00 00 | 6.0 |
| S68FIR | 18 27 17.5 | 01 13 23 | 8.0 |
| S68N | 18 27 15.9 | 01 14 49 | 9.0 |

TABLE 3
DEUTERO–AMMONIA MICROTURBULENT COLUMN DENSITY FITS

| Source | $\Delta V$ km s$^{-1}$ | $T_r^* \Delta V$ K km s$^{-1}$ | $T_K$[†] K | $n(H_2)$[†] 10$^6$ cm$^{-3}$ | N(NH$_2$D) 10$^{12}$ cm$^{-2}$ | Temp. Ref. |
|---|---|---|---|---|---|---|
| L1448 IRS2 | 0.49 | 0.84 ± 0.07 | 20 | 0.1 | 7.60 ± 0.61 | O'Linger et al. 1999 |
| L1448 NW | 1.38 | 3.01 ± 0.60 | 30 | 0.1 | 36.0 ± 7.20 | Barsony et al. 1998 |
| L1448 IRS3 | 1.10 | 1.39 ± 0.09 | 20–50 | 0.1-5 | 8.14 ± 0.55 | This paper |
| L1448 C | 0.93 | 0.81 ± 0.26 | 40 ± 10 | 1 | 9.30 ± 2.96 | This paper |
| NGC 1333 DCO$^+$ | 2.60 | 3.77 ± 0.96 | 20 | 0.6 | 45.0 ± 11.5 | This paper |
| NGC 1333 IRAS2 | 1.31 | 0.46 ± 0.09 | 20–85 | 0.4-1.26 | 2.62 ± 0.49 | Wootten et al. 1999 |
| NGC 1333 IRAS7 | 2.31 | 2.30 ± 0.46 | 40 | 0.3 | 2.60 ± 0.52 | Lefloch et al. 1998 |
| NGC 1333 IRAS4A[1] | 1.50 | 3.98 ± 1.19 | 25–50 | 0.7-2 | 21.8 ± 6.50 | Wootten et al. 1999 |
| NGC 1333 IRAS4C | 1.10 | 1.87 ± 0.11 | 15 | 0.1 | 15.4 ± 0.90 | This paper |
| IRAS 03282 | 0.90 | 0.76 ± 0.23 | 20 | 0.1 | 7.00 ± 2.12 | Wootten et al. 1999 |
| L1551 | 1.35 | 1.04 ± 0.11 | 50 | 0.1 | 22.5 ± 2.40 | Wootten et al. 1999 |
| TMC1 AM | 1.12 | 0.44 ± 0.12 | 10 | 0.1 | 9.77 ± 2.57 | This paper |
| L1544 | 0.96 | 2.76 ± 0.12 | 10 | 0.3 | 26.0 ± 1.10 | This paper |
| OMC2 | 1.66 | 2.55 ± 0.37 | 20 | 0.1 | 220.0 ± 32.0 | Batrla et al. 1983 |
| HH1 | 1.68 | 1.04 ± 0.33 | 15 | 0.1 | 100.0 ± 32.0 | Martin–Pint. (1987) |
| NGC 2264 | 3.10 | 0.41 ± 0.08 | 25 | 0.1 | 34.4 ± 5.20 | de Bois. et al. 1996 |
| L183 | 0.30[2] | 2.40 ± 0.42 | 10 | 0.01 | 30.0 ± 11.1 | This paper |
| VLA 1623 | 1.04 | 1.92 ± 0.17 | 20 | 0.1 | 17.0 ± 1.50 | AWB93 |
| Oph B2 | 1.33 | 1.90 ± 0.40 | 13 | 0.1 | 9.00 ± 1.89 | Lefloch et al. 1998 |
| IRAS 16293 | 0.81 | 1.24 ± 0.12 | 30 | 0.6 | 4.50 ± 0.30 | van Dish. et al. 1995 [‡] |
| L1689N | 1.22 | 6.46 ± 0.45 | 8 | 0.1 | 160.0 ± 11.0 | Wootten (pc) |
| S68 FIR | 1.58 | 1.23 ± 0.43 | 20–100 | 0.3-1.26 | 34.0 ± 12.00 | McMullin et al. 1999 |
| S68N | 1.46 | 1.32 ± 0.15 | 15–75 | 0.3-2 | 7.82 ± 0.87 | McMullin et al. 1999 |

[†]Sources with two values list the H$_2$CO fits for density and temperature in two layer models

[‡]From the fit to their cold, extended layer

[1]The error listed contains an estimate to the error in the linewidth of 0.3 km s$^{-1}$.

[2]Using line fits from high resolution 30 kHz spectrum.

TABLE 4
NH$_2$D $5\sigma$ UPPER LIMITS

| Source | $T_r^*\Delta V$ K km s$^{-1}$ | N(NH$_2$D) cm$^{-2}$ |
|---|---|---|
| IC 348 | 0.094 | $2 \times 10^{12}$ |
| L1512 | 0.024 | $1 \times 10^{12}$ |
| TMC1 CY | 0.007 | $5 \times 10^{11}$ |
| Oph B1 | 0.045 | $1 \times 10^{12}$ |
| L63 | 0.060 | $1.5 \times 10^{12}$ |

[‡]N.B. Upper limits from $T_K = 20K$ and $n(H_2) = 1 \times 10^5$

TABLE 5
AMMONIA MICROTURBULENT COLUMN DENSITY FITS

| Source[†] | $\Delta V$ km s$^{-1}$ | $T_r^*\Delta V$ K km s$^{-1}$ | $T_K$[‡] K | $n(H_2)$[†] $10^6$ cm$^{-3}$ | N(NH$_3$) $10^{14}$ cm$^{-2}$ | Ref. |
|---|---|---|---|---|---|---|
| L1448 IRS2 | 0.87 | $6.21 \pm 1.32$ | 20 | 1 | $3.23 \pm 0.69$ | This paper |
| L1448 NW | | | | | $2.00 \pm 0.20$ | Barsony et al. 1998 |
| L1448 IRS3 | 1.22 | $14.74 \pm 0.74$ | 20–50 (30) | 0.1-5 | $4.53 \pm 0.23$ | This paper |
| L1448 C | 1.37 | $11.07 \pm 2.35$ | $40 \pm 10$ | 1 | $3.23 \pm 0.69$ | This paper |
| NGC 1333 DCO$^+$ | 1.56 | $15.07 \pm 1.56$ | < 30 (38) | 0.6 | $3.71 \pm 0.38$ | This paper |
| NGC 1333 IRAS4A | 1.52 | $12.09 \pm 1.61$ | 25–50 | 0.7-2 | $3.08 \pm 0.41$ | Blake et al. 1995 |
| NGC 1333 IRAS4C | 1.44 | $9.73 \pm 3.50$ | 25 (40) | 0.1 | $2.30 \pm 0.82$ | This paper |
| IRAS 03282[†] | | | | | $10.0 \pm 2.0$ | BMP91 |
| IC 348[†] | | | | | $2.50 \pm 1.50$ | BGK87 |
| L1551 | 1.27 | 0.78 | 5.33 | 0.1 | $2.60 \pm 0.26$ | This paper |
| TMC1 NH$_3$ | 0.81 | $5.48 \pm 1.37$ | 20 | 0.1 | $1.55 \pm 0.39$ | Pratap et al. 1997 |
| TMC1 CY | 0.72 | $3.34 \pm 0.45$ | 20 | 0.1 | $0.91 \pm 0.12$ | Pratap et al. 1997 |
| L1512[†] | | | | | 7.94 | BM83 |
| L1544 | 0.73 | $5.04 \pm 0.89$ | 10 | 0.3 | $1.97 \pm 0.35$ | This paper |
| OMC2[†] | | | | | $75.9 \pm 8.0$ | CW94 |
| HH1[†] | | | | | $5.00 \pm 0.38$ | MP87 |
| NGC 2264[†] | | | | | 8.00 | Krügel et al. 1996 |
| L183 | 0.73 | $7.52 \pm 1.45$ | 10 | 0.01 | $5.19 \pm 0.91$ | Olberg et al. 1983 |
| VLA1623[†] | | | | | 2.00 | Wootten et al. 1999 |
| Oph B1[†] | | | 19 | | $3.45 \pm 1.75$ | MP83,ZBW84 |
| Oph B2 | 1.20 | 4.08 | 13 | 0.1 | 0.96 | MP83 |
| IRAS 16293[†] | | | | | $15.0 \pm 5.0$ | Mundy et al. 1995 |
| L1689N | 1.00 | 0.55 | 8 | 1 | 18.0 | Wootten (pc) |
| L63[†] | | | | | 10.0 | BM83 |
| S68 FIR | 1.25 | $8.83 \pm 2.33$ | 20–100 | 0.3-1.3 | $2.71 \pm 0.72$ | This paper |
| S68N | 1.24 | $5.17 \pm 0.77$ | 15–75 | 0.3-2 | $1.45 \pm 0.22$ | This paper |

[†]NH$_3$ column densities for Sources without listed line parameters are taken from the noted references.

[‡]Sources with two values list the density and temperature in two layer models

[1]MP83=Martin-Pintado, Wilson, Gardner, & Henkel (1983)

[2]ZBW84=Zeng, Batrla, & Wilson (1984)

[3]MP87=Martin-Pintado & Cernicharo (1987)

[4]BM83=Benson & Myers (1983)

[5]CW94=Cesaroni & Wilson (1994)

[6]BGK87=Bachiller, Guillateau, & Kahane (1987)

[7]BMP91=Bachiller, Martin-Pintado, & Planesas (1991)

TABLE 6

AMMONIA FRACTIONATION FOR SINGLE TEMPERATURE AND DENSITY MODELS

| Source | $T_K$ K | $n(H_2)$ cm$^{-3}$ | NH$_2$D/NH$_3$ |
|---|---|---|---|
| L1448 IRS2 | 20 | $1 \times 10^6$ | $0.024 \pm 0.005$ |
| L1448 NW | 30 | $1 \times 10^6$ | $0.09 \pm 0.02$ |
| L1448 C | $40^{+30}_{-10}$ | $1 \times 10^6$ | $0.029 \pm 0.006$ |
| NGC 1333 DCO$^+$ | $< 30$ | $1 \times 10^6$ | $0.10 \pm 0.03$ |
| NGC 1333 IRAS4C | 25 | $1 \times 10^6$ | $0.067 \pm 0.013$ |
| IRAS 03282 | 20 | $1 \times 10^5$ | $0.007 \pm 0.003$ |
| L1551 | 50 | $7 \times 10^5$ | $0.087 \pm 0.013$ |
| TMC1 NH$_3$ | 20 | $1 \times 10^5$ | $0.06 \pm 0.02$ |
| L1544 | 10 | $1 \times 10^5$ | $0.13 \pm 0.02$ |
| OMC 2[2] | 20 | $1 \times 10^5$ | $0.029 \pm 0.006$ |
| HH1 | 15 | $1 \times 10^5$ | $0.074 \pm 0.024$ |
| NGC 2264[1] | 25 | $1 \times 10^5$ | $0.043 \pm 0.007$ |
| L183 | 10 | $1 \times 10^4$ | $0.058 \pm 0.010$ |
| VLA 1623 | 20 | $1 \times 10^6$ | $0.085 \pm 0.008$ |
| Oph B2[3] | 13 | $1 \times 10^5$ | $0.090 \pm 0.019$ |
| IRAS 16293 | 30 | $6 \times 10^5$ | $0.0028 \pm 0.001$ |
| L1689N | 8 | $1 \times 10^5$ | $0.089 \pm 0.006$ |

[1]NH$_3$ data from Krügel et al. (1996).

[2]NH$_3$ data from Cesaroni & Wilson (1994)

[3]Martin–Pintado et al. 1983

TABLE 7

MULTI–LAYER MODELS OF AMMONIA DEUTERATION

| Source | $n$ cm$^{-3}$ | $T$ K | NH$_2$D/NH$_3$[1] |
|---|---|---|---|
| NGC 1333 IRAS4A | $7 \times 10^5$ | 25 | 0.07 |
| | $2 \times 10^6$ | 50 | |
| S68 FIR | $3 \times 10^5$ | 20 | 0.13 |
| | $1.26 \times 10^6$ | 100 | |
| S68N | $3 \times 10^5$ | 15 | 0.05 |
| | $2 \times 10^6$ | 75 | |
| L1448 IRS3 | $1 \times 10^5$ | 20 | 0.02 |
| | $5 \times 10^6$ | 50 | |

[1]Summed over both layers.

TABLE 8
NH$_2$D Ortho–Para Ratio

| Source | $\int T_{\rm A}\,dv$(110 GHz) K km s$^{-1}$ | $\int T_{\rm A}\,dv$(86 GHz) K km s$^{-1}$ | $\frac{\int T_{\rm A}\,dv(86GHz)}{\int T_{\rm A}\,dv(110GHz)}$ | $\frac{\rm N(86GHz)}{\rm N(110GHz)}$ |
|---|---|---|---|---|
| N1333 | $0.598 \pm 0.142$ | $2.447 \pm 0.623$ | $4.09 \pm 1.43$ | $4.11 \pm 1.30$ |
| L1544 | $0.295 \pm 0.144$ | $1.792 \pm 0.075$ | $6.08 \pm 2.98$ | $6.10 \pm 3.02$ |
| OMC2 | $0.90 \pm 0.13$ | $1.66 \pm 0.24$ | $1.84 \pm 0.38$ | $1.84 \pm 0.90$ |
| HH1 | $0.41 \pm 0.15$ | $0.68 \pm 0.21$ | $1.66 \pm 0.79$ | $1.66 \pm 0.92$ |
| L183 | $0.40 \pm 0.06$ | $1.56 \pm 0.27$ | $3.95 \pm 0.92$ | $3.96 \pm 0.92$ |
| OPHB2 | $0.42 \pm 0.11$ | $1.23 \pm 0.26$ | $2.94 \pm 1.01$ | $2.95 \pm 1.20$ |
| L1689N | $1.59 \pm 0.21$ | $4.19 \pm 0.29$ | $2.63 \pm 0.39$ | $2.64 \pm 0.45$ |
| L1551 | $0.30 \pm 0.24$ | $0.69 \pm 0.07$ | $2.31 \pm 1.85$ | $2.31 \pm 1.80$ |

TABLE 9
Ammonia Deuteratium Fractionation

| Source | $T_K$[K] | NH$_2$D/NH$_3$ | DCO$^+$/HCO$^{+\dagger}$ | DCN/HCN$^\dagger$ |
|---|---|---|---|---|
| L1448 IRS2 | 20 | $0.024 \pm 0.005$ | $\cdots$ | $\cdots$ |
| L1448 NW | 30 | $0.09 \pm 0.02$ | $\cdots$ | $\cdots$ |
| L1448 IRS3 | 20 | $0.018 \pm 0.001$ | $\cdots$ | $\cdots$ |
| L1448 C | 40 | $0.029 \pm 0.011$ | $\cdots$ | $\cdots$ |
| NGC 1333 DCO$^+$ | 30 | $0.10 \pm 0.03$ | $0.024^1$ | $\cdots$ |
| NGC 1333 IRAS4A | 25–50 | $0.071 \pm 0.023$ | $\cdots$ | $\cdots$ |
| NGC 1333 IRAS4C | 15 | $0.067 \pm 0.024$ | $\cdots$ | $\cdots$ |
| IRAS 03282 | 20 | $0.007 \pm 0.003$ | $\cdots$ | $\cdots$ |
| IC 348 | 20 | $< 0.008$ | $\cdots$ | $\cdots$ |
| L1551 | 50 | $0.087 \pm 0.013$ | $0.035^1$ | $0.016 \pm 0.001^3$ |
| TMC1 AM | 10 | $0.06 \pm 0.02$ | $0.027^2$ | $0.022^3$ |
| TMC1 CY | 10 | $< 0.006$ | $0.00004$ | $\cdots$ |
| L1512 | 20 | $< 0.006$ | $\cdots$ | $\cdots$ |
| L1544 | 10 | $0.13 \pm 0.02$ | $0.12 \pm 0.02$ | $\cdots$ |
| OMC2 | 20 | $0.029 \pm 0.006$ | $\cdots$ | $0.01^3$ |
| HH1 | 15 | $0.074 \pm 0.024$ | $\cdots$ | $\cdots$ |
| NGC 2264 | 25 | $0.043 \pm 0.007$ | $0.017^1$ | $\cdots$ |
| L183 | 10 | $0.058 \pm 0.010$ | $0.07^1$ | $\cdots$ |
| VLA1623 | 20 | $0.085 \pm 0.008$ | $\cdots$ | $\cdots$ |
| Oph B1 | 19 | $< 0.003$ | $\cdots$ | $\cdots$ |
| OPH B2 | 13 | $0.09 \pm 0.02$ | $\cdots$ | $0.013$ |
| IRAS 16293 | 30 | $0.003 \pm 0.001$ | $\cdots$ | $\cdots$ |
| L1689N | 8 | $0.089 \pm 0.006$ | $\cdots$ | $\cdots$ |
| L63 | 20 | $< 0.002$ | $\cdots$ | $\cdots$ |
| S68 FIR | 20–100 | $0.126 \pm 0.055$ | $0.005$ | $0.010$ |
| S68N | 15–75 | $0.054 \pm 0.010$ | $\cdots$ | $0.009$ |

$^\dagger$Assumes $^{12}$C/$^{13}$C $= 60$

[1]Williams et al. 1998

[2]Butner et al. 1995

[3]Greason 1986

TABLE 10
Observed Asymmetries

| Source | NH$_2$D[a] $J = 1_{11} \to 1_{01}$ | Skewness | CS $J = 2 \to 1$[b] | H$_2$CO $J = 2_{12} \to 1_{11}$[b] | HCO$^+$ $J = 3 \to 2$[c] | HCO$^+$ $J = 4 \to 3$[c] |
|---|---|---|---|---|---|---|
| L1448C | Blue | $-0.014 \pm 0.004$ | Blue | Red | Red | Red |
| IRAS4A | Blue | $-0.38 \pm 0.09$ | Blue | Blue | Blue | Blue |
| IRAS4C | Blue | $-0.010 \pm 0.004$ | $\cdots$ | $\cdots$ | $\cdots$ | $\cdots$ |
| L1551 IRS5 | None | $\cdots$ | None | Red | None | None |
| S68N | Blue | $-0.704 \pm 0.194$ | None | Blue | None | None |
| S68 FIR | Red?[d] | $\cdots$ | Blue | Red | Red | Blue |

[a]This paper; only the 86 GHz data displays these asymmetries

[b]Mardones et al. (1997)

[c]Gregersen et al. (1997)

[d]This is a fit by eye, not by a strict Gaussian fit to the line features